Folded cavity SOI microring sensors for high sensitivity and real time measurement of biomolecular binding

D.-X. Xu[1*], A. Densmore[1], A. Delâge[1], P. Waldron[1], R. McKinnon[1], S. Janz[1], J. Lapointe[1], G. Lopinski[2], T. Mischki[2], E. Post[1], P. Cheben[1] and J. H. Schmid[1]

[1] *Institute for Microstructural Sciences, National Research Council of Canada, 1200 Montreal Rd., Ottawa, Ontario, Canada, K1A 0R6*
[2]*Steacie Institute for Molecular Sciences, National Research Council of Canada, 100 Sussex Dr., Ottawa, Ontario, Canada, K1A 0R6*
[*]*Corresponding author: Danxia.Xu@nrc-cnrc.gc.ca*

Abstract: We demonstrate folded waveguide ring resonators for biomolecular sensing. We show that extending the ring cavity length increases the resonator quality factor, and thereby enhances the sensor resolution and minimum level of detection, while at the same time relaxing the tolerance on the coupling conditions to provide stable and large resonance contrast. The folded spiral path geometry allows a 1.2 mm long ring waveguide to be enclosed in a 150 μm diameter sensor area. The spiral cavity resonator is used to monitor the streptavidin protein binding with a detection limit of ~3 pg/mm^2, or a total mass of ~ 5 fg. The real time measurements are used to analyze the kinetics of biotin-streptavidin binding.

OCIS codes: (130.3120) Integrated optics devices; (220.0220) Optical design and fabrication; (230.5750) Resonators; (130.6010) Sensors; (120.0120) Instrumentation, measurement, and metrology.

References and links

1. J. Homola, S. S. Yee, and G. Gauglitz, "Surface plasmon resonance sensors: review," Sens. Actuators B **54**, 3–15 (1999).
2. R. Karlsson, "SPR for molecular interaction analysis: a review of emerging application areas," J. Mol. Recognit. **17**, 151–161 (2004).
3. O. Lazcka, F. J. Del Campo, and F. X. Muñoz, "Pathogen detection: A perspective of traditional methods and biosensors," Biosens. Bioelectron. **22**, 1205-1217 (2007).
4. A. M. Armani, R. P. Kulkarni, S. E. Fraser, R. C. Flagan and K. J. Vahala, "Label-free, single-molecule detection with optical microcavities," Science **317**, 783-787 (2007).
5. B. J. Luff J. S. Wilkinson, J. Piehler, U. Hollenback, J. Ingenhoff, and N. Fabricius, "Integrated optical Mach-Zehnder biosensor," J. Lightwave Technol. **16**, 583-591 (1998).
6. F. Prieto, B. Sepulveda, A. Calle, A Llobera, C. Dominguez, A. Abad, A. Montoya, and L. M. Lechuga, "An integrated optical interferometric nanodevice based on silicon technology for biosensor applications," Nanotechnology **14**, 907-912 (2003).
7. G. P. Anderson, J. P. Golden and F. S. Ligler, "A fiber optic biosensor: combination tapered fibers designed for improved signal acquisition," Biosens. Bioelectron. **8**, 249-256 (1993).
8. A. Densmore, D.-X. Xu, P. Waldron, S. Janz, P. Cheben, J. Lapointe, A. Delâge, B. Lamontagne, J. H. Schmid, and E. Post, "A silicon-on-insulator photonic wire based evanescent field sensor," IEEE Photon. Technol. Lett. **18**, 2520-2522 (2006).
9. K. De Vos, I. Bartolozzi, E. Schacht, P. Bienstman, and R. Baets, "Silicon-on-insulator microring resonator for sensitive and label-free biosensing," Opt. Express **15**, 7610-7615 (2007).
10. D.-X. Xu, A. Densmore, J. Lapointe, P. Waldron, P. Cheben, A. Delâge, B. Lamontagne, S. Janz, J. H. Schmid and E. Post, "High Index Contrast Photonic Waveguide Components for Biological Sensing", Symposium "Biomedical and Clinical Sensors," paper # 2096, ECS 2006 Joint International Meeting, Oct. 29 – Nov. 3, 2006, Cancun, Mexico.

#97938 - $15.00 USD Received 25 Jun 2008; revised 30 Aug 2008; accepted 8 Sep 2008; published 11 Sep 2008

11. A. Densmore, D. X. Xu, P. Waldron, S. Janz, A. Delâge, J. Lapointe and P. Cheben, "Thin silicon waveguides for biological and chemical sensing," Proc. SPIE Photonics West 2007, paper 6477-43, San Jose, CA, Jan. 20-25, 2007.
12. A. Ksendzov, M. L. Homer, and A. M. Manfreda, "Integrated optics ring-resonator chemical sensor with polymer transduction layer," Electron. Lett. **40**, 63-65 (2004).
13. A. Yalcin, K.C. Popat, J. C. Aldridge, T. A. Desai, J. Hryniewicz, N. Chbouki, B. E. Little, O. King, V. Van, S. Chu, D. Gill, M. Anthes-Washburn, M. S. Unlu and B. B. Goldberg, "Optical sensing of biomolecules using microring resonators," IEEE J. Sel. Top. Quantum. Electron. **12**, 148-155 (2006).
14. W. Lukosz, "Principles and sensitivities of integrated optical and surface plasmon sensors for direct affinity sensing and immunosensing," Biosens. Bioelectron. **6**, 215-225 (1991).
15. A. Yariv, "Universal relations for coupling of optical power between microresonators and dielectric waveguides," Electron. Lett. **36**, 321-323 (2000).
16. K. Okamoto, *Fundamentals of optical waveguides*, (Academic Press, Elsevier 2006) p. 199.
17. L. F. Stokes, M. Chodorow and H. J. Shaw, "All-single-mode fiber resonator," Optics Lett. **7**, 288-290 (1982).
18. D.-X. Xu, A. Densmore, P. Waldron, J. Lapointe, E. Post, A. Delâge, S. Janz, P. Cheben, J. Schmid and B. Lamontagne, "High bandwidth SOI photonic wire ring resonators using MMI couplers," Opt. Express **15**, 3149-3155 (2007).
19. A. Densmore, D.-X. Xu, S. Janz, P. Waldron, T. Mischki, G. Lopinski, A. Delâge, J. Lapointe, P. Cheben, B. Lamontagne and J. H. Schmid, "Spiral-path high-sensitivity silicon photonic wire molecular sensor with temperature-independent response," Opt. Lett. **6**, 596-598 (2008).
20. J. Bishop, A. Chagovetz, and S. Blair, "Effects of fill fraction on the capture efficiency of nanoscale molecular transducers," Nanotechnology **17**, 2442-2448 (2006).
21. D.-X. Xu, S. Janz, and P. Cheben, "Design of polarization-insensitive ring resonators in silicon-on-insulator using MMI couplers and cladding stress engineering," IEEE Photon. Technol. Lett. **18**, 343-345 (2006).
22. S. Xiao, M. H. Khan, H. Shen and M. Qi, "Modeling and measurement of losses in silicon- on-insulator resonators and bends," Opt. Lett. **15**, 10553-10561 (2007).
23. J. Spinke, M. Liley and F.-J. Schmitt, "Molecular recognition at self-assembed monolayers: optimization of surface functionalization," J. Chem. Phys. **99**, 7012-7019 (1993).
24. L. S. Jung, C. T. Campbell, T. M. Chinowsky, M. N. Mar and S. S. Yee, "Quantitative interpretation of the response of surface plasmon resonance sensors to adsorbed films," Langmuir **14**, 5636-5648 (1998).
25. J. Štěpánek, H. Vaisocherová and M. Piliarik, "Molecular interactions in SPR sensors," Surface Plasmon Resonance based Sensors, J. Homola, ed., Springer Ser Chem Sens Biosens **4**, 69-91 (2006).
26. D. E. Hyre, I. Le Trong, E. A. Merritt J. F. Eccleston, N. M. Green, R. E. Stenkamp, and P. S. Stayton, "Cooperative hydrogen bond interactions in the streptavidin biotin system," Protein Science **165**, 569-67 (2006).

1. Introduction

The selective binding of one biomolecule to another is the basis of most of the chemical regulatory processes necessary to maintain life. Therefore, efforts to measure biomolecular interactions occupy a central place in biochemical and molecular biological research and development. Reliable assays are essential to applications such as drug discovery, environmental monitoring, crop and food protection. In many of these applications, quantitative and real-time monitoring of the molecular interaction is essential.

The experimental techniques available for real time monitoring of molecular interactions are rather limited. The most commercially successful method is the surface plasmon resonance (SPR) based on probing the surface with a propagating surface plasmon wave [1-3]. There has been ongoing effort to miniaturize the SPR instrument, and to develop SPR with higher channel count to increase the screening throughput. However, SPR measurement apparatus remains complex and expensive [3]. Furthermore the measurement accuracy of SPR has a fundamental limit set by the short propagation length of the surface plasmon [1].

Evanescent field (EVF) dielectric waveguide sensing is another method that has been used for two decades for similar applications, and provides similar information as the SPR [4 – 8]. Planar waveguide EVF sensors provide significant reduction in sensor size as compared to fibre sensors [7], particularly for waveguides based on high index contrast materials [6, 8, 9], making them amendable to integration for more robust operation, more rapid and multiplexed analysis with high channel count assays, and feasibility for volume production.

Several types of photonic waveguide devices have been used to measure the phase change caused by the surface adsorption with varying degrees of accuracy. To achieve high sensitivity, sensor optimization should be approached from two aspects. First the magnitude of response for a given surface perturbation should be maximized, which is primarily

#97938 - $15.00 USD Received 25 Jun 2008; revised 30 Aug 2008; accepted 8 Sep 2008; published 11 Sep 2008

achieved by proper choice of the waveguide material and cross-section. Secondly the accuracy of measurement for a given response should be optimized, by sensing circuit design optimization. Ring resonator sensors made in SOI [9 – 11], polymer [12] and silicon nitride [13] materials have been reported, using different designs and interrogation methods. Compared to devices such as Mach-Zehnder interferometer and grating couplers, ring resonators are compact, highly sensitive, and array compatible. On the other hand, ring resonators are very sensitive to small dimensional variations, hence more challenging to fabricate. We present the design, analysis and experimental demonstration of a novel folded cavity wire ring resonator sensor made in SOI for real time monitoring of biomolecule interaction. Shrinking the Si waveguide cross-section to submicron dimensions enhances the intrinsic response of the sensor to the surface perturbation [8]. A long sensing cavity length folded in a small area increases the sensor quality factor, relaxes the resonance matching condition, and increases the signal contrast ratio, while maintaining a compact device footprint. The consideration of robust and reproducible performance is particularly important for multi-sensor arrays used for the cancellation of contributions from non-specific binding and environmental variations, where the reference and the sensing elements are required to be nominally identical. When employing ring resonators with long cavities, compatibility with microfluidic delivery and functionalization spotters are also important considerations for practical sensors. Efficient molecular capture from the fluidic flow is another issue for the sensing function. All these requirements can benefit from the folded waveguide configuration that occupies a small area which intercepts most of the microfluidic channel width.

2. Theory

The transduction signal in EVF waveguide biosensors is a cumulative optical phase delay $\Delta\theta = (2\pi/\lambda)\ \Delta n_{eff} L$, which is proportional to the waveguide effective index perturbation (Δn_{eff}) caused by the molecule adsorption on the surface, and the interaction length L between the sensing medium and the waveguide. Here λ is the wavelength in vacuum. The effective index perturbation in a waveguide Δn_{eff} increases with the fraction of the optical field interacting with the molecules residing on the sensor surface [8, 14]. Using high index contrast SOI waveguides with sub-micron dimensions, the evanescent field is highly concentrated above the waveguide core, as shown in Fig. 1(a) for the transverse magnetic (TM) mode. The SOI sensor exhibits a high response Δn_{eff} to both the surface adsorption and bulk index change, and the response to the surface adsorption of a 4 nm thick molecular layer as a function of core thickness is shown in Fig. 1(c). The maximum response of the SOI waveguide sensor is approximately two orders of magnitude higher than that in the glass waveguides (or fibers). These findings are supported by our experimental sensing results using silicon wire waveguide sensors that have been reported previously [8, 10, 11]. A native silicon surface is prone to oxidation in air or aqueous solutions. The dashed line in Fig. 1(c) indicates that there is only a minimum penalty in sensitivity upon depositing a thin layer of oxide on the silicon surface. We have included a thin oxide layer in our sensors to improve the sensor stability, while also enabling the use of standard silane chemistry for surface functionalization.

#97938 - $15.00 USD Received 25 Jun 2008; revised 30 Aug 2008; accepted 8 Sep 2008; published 11 Sep 2008

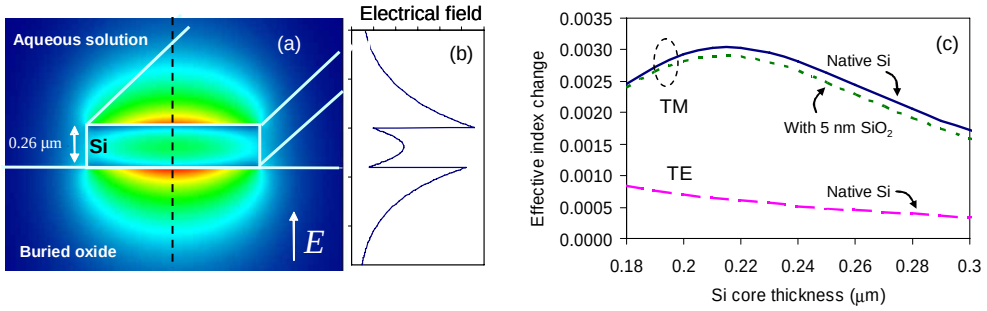

Fig. 1. (a). Cross section of a 0.26 μm × 0.45 μm SOI photonic wire waveguide, and the corresponding electric field distribution for the TM polarization; (b) Line plot across the dashed line in (a); (c) Sensor response in term of the effective index change Δn_{eff} due to a 4 nm organic layer (n = 1.5) for the TE and TM polarizations on a native silicon surface, and the response on a surface with 5 nm of capping oxide for TM.

Figures 2(a), 2(b) illustrate a simple race-track ring and the proposed spiral ring resonator design, with short and long cavity length respectively. The coupling between the bus waveguide and the ring cavity is characterized by a cross coupling coefficient κ and a through coupling ratio $t = (1 - \kappa^2)^{1/2}$. The loss factor α gives the field attenuation after one round trip through the ring cavity waveguide (i.e. no loss corresponds to $\alpha = 1$). The normalized transmission intensity at the bus waveguide output is [15]:

$$I = \left[\frac{\alpha^2 - 2\alpha t \cos\theta + t^2}{1 - 2\alpha t \cos\theta + \alpha^2 t^2} \right] \tag{1}$$

where $\theta = 2\pi n_{eff} L/\lambda$ is the round trip phase, and L is the cavity length. The free spectral range $FSR = \lambda^2/n_g L$, and it decreases with the cavity length L. Here n_g is the ring waveguide effective group index.

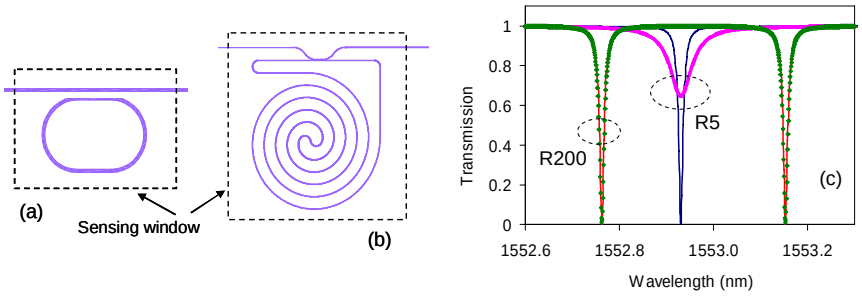

Fig. 2. Schematics of sensors made of (a) a race-track cavity ring; and (b) a spiral cavity ring; (c) Transmission spectra for the R5 and R200 ring resonators under different matching conditions. R5 ring: $t = \alpha$ (solid blue line), $t = 0.99\alpha$ (magenta symbols). R200 ring: $t = \alpha$ (solid red line), $t = 0.99\alpha$ (green symbols).

The sharpness of the resonance peaks is usually expressed in terms of the quality factor Q:

$$Q \equiv \frac{\lambda}{\Delta\lambda_{FWHM}} = \frac{\pi n_g L}{\lambda} [\arccos(\frac{2\alpha t}{1+\alpha^2 t^2})]^{-1} \tag{2}$$

#97938 - $15.00 USD Received 25 Jun 2008; revised 30 Aug 2008; accepted 8 Sep 2008; published 11 Sep 2008

where $\Delta\lambda_{FWHM}$ is the resonance full-width-at-half-maximum. Equation (2) is directly derived from Eq. (1) without approximation. Traditionally, Q factor is used to describe resonators with low damping (or low loss and low coupling factor in the case of optical resonators). When $\alpha t \sim 1$, Eq. (2) can be approximated by the more familiar form of [16, 17]:

$$Q \cong \frac{\pi n_g L}{\lambda} \frac{\sqrt{\alpha t}}{1-\alpha t} \tag{3}$$

which we had previously used [18]. By rigorously applying the definition of Q to be $Q \equiv \lambda/\Delta\lambda_{FWHM}$, this figure-of-merit can be extended to higher damping conditions as a useful indicator of the resonance linewidth. The dependence of Q on the structural parameters is better described by Eq. (2) over the entire range of αt from zero to unity.

In sensing applications, the mode effective index change Δn_{eff} caused by the adsorption of molecules can be obtained by measuring the corresponding resonance wavelength shift $\Delta\lambda$:

$$\Delta\lambda = \lambda \frac{\Delta n_{eff}}{n_g} \tag{4}$$

which is independent of the cavity length. It is important to note that the use of n_g in Eq. (2 - 4) takes into account the effective index dispersion, which is particularly important for Si wire waveguides. The minimum resolvable wavelength shift depends on the linewidth of the resonance $\Delta\lambda_{FWHM}$, so a high Q is desirable. On the other hand, a large resonance contrast η (defined as $\eta = (I_{max} - I_{min})/(I_{max} + I_{min})$) is also important for high signal to noise ratio measurements. This figure-of-merit can also be represented by the extinction ratio $ER = I_{max}/I_{min}$. The largest contrast occurs when the coupling coefficient t satisfies the critical coupling condition $t = \alpha$ for which the transmission on resonance is zero, η is unity, and ER is infinite. It can be observed from Eq. (1) that the ring sensor performance can be optimized by reducing waveguide loss to increase Q, and adjusting the coupling t accordingly such that $\alpha = t \approx 1$. On the other hand, the quality factor also increases with the cavity length L. We will illustrate below the limitations of a short cavity and low loss resonator for practical implementations.

In the following, we calculate the properties of resonators constructed of waveguides with a cross section of $0.26 \times 0.45\ \mu m^2$ ($n_{eff} \approx 2.2$, $n_g \approx 4.8$), as used in our experiments. The Si thickness of 0.26 μm was chosen to ensure proper guiding in waveguides with SU8, water and air upper claddings as encountered in the sensor structure. The ring resonators have cavity lengths of 31.4 μm (radius of 5 μm, referred to as R5 ring hereafter) and 1256.6 μm (radius of 200 μm, referred to as R200 ring), respectively. The transmission spectra calculated using Eq. (1) are shown in Fig. 2(c), for the coupling conditions of $t = \alpha$ and $t = 0.99\alpha$, respectively. The cavity loss factor α is assumed to scale linearly with the cavity length: $\alpha = 10^{sL/20} + \alpha_C$. Here s is the scaling factor and is taken as $s = -3$ dB/cm for these calculations. This is a reasonable assumption when the waveguide bend loss is not a significant source of the cavity loss, as usually is the case for SOI wire waveguides. The coupler loss α_C is assumed to be zero. These resonance curves show that the Q factors and contrast ratio for short rings (i.e. R5) deteriorate rapidly with even small changes in the coupling. Using a longer cavity (i.e. R200), the resonator is much less sensitive to the same coupling change, with the two resonance curves nearly overlap. The FSR is 14.6 nm and 0.38 nm for the R5 and R200 resonators, respectively.

The calculated variation of the quality factor Q with the cavity length L and coupling conditions are shown in Fig. 3(a), for a wavelength of λ=1520 nm and again for a cavity waveguide loss scaling factor of $s = -3$ dB/cm. Three coupling conditions are considered, i.e. $t = (1, 0.99, 0.95)\alpha$, and the results for the R5 and R200 rings are summarized in Table I. For the short cavity (R5) resonator, a 5% variation in the coupling coefficient caused Q to decrease from 143,600 to 5,800. In the R200 resonator, the corresponding Q values are much

#97938 - $15.00 USD Received 25 Jun 2008; revised 30 Aug 2008; accepted 8 Sep 2008; published 11 Sep 2008

less sensitive, changing from 143,800 to 90,650 for the same coupling parameter change. Furthermore, the Q for R200 ring is higher than that for the R5 ring for all the coupling conditions even though the corresponding α is smaller, so there is an advantage in Q for using longer cavities. For experimentally verifying these relations, a simple approach is to keep the same coupler design (i.e. a constant t) and vary the cavity length L. The dependence of Q on the cavity length L for the case of t = 0.707 (i.e. 50:50 power splitting ratio) is shown in Fig. 3(c) for comparison with experiments below. Similarly, the Q increases with L. The dependence of the resonance contrast η is shown in Fig. 3(b) for t = (1, 0.99, 0.95)α. When t = α, all resonators have full contrast and η =1. The magnitude of η increases as t approaches α, and it also increases with L. Further details are listed in Table 1.

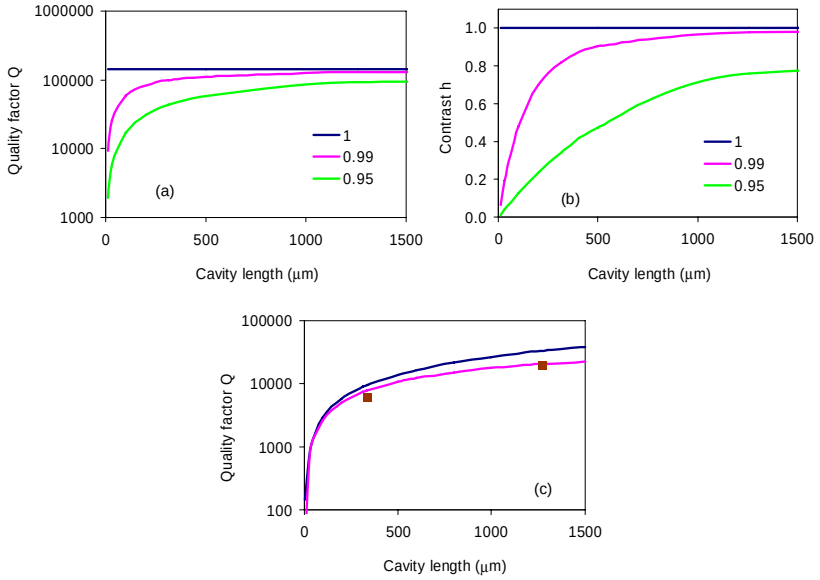

Fig. 3. (a). Quality factor Q as a function of the cavity length L for four matching conditions t = (1, 0.99, 0.95)α; (b) Resonance contrast as a function of the cavity length L for the corresponding matching conditions.; (c) Quality factor Q as a function of the cavity length L for t = 0.707 and a loss factor of −3 dB/cm (blue line) and −22 dB/cm (magenta line). The symbols are the measured Q values for the simple race-track ring (L=336 μm) and the spiral ring (L=1.27 mm).

Table I. Resonator figures-of-merit for the R5 and R200 resonators under different α and t matching conditions, assuming a cavity loss of 3 dB/cm.

Design	Cavity length (μm)	Matching condition	Coupling coefficient t	Quality factor Q	Contrast η	Extinction ratio (dB)
R5	31.4	t = α	0.9988	143,600	100%	∞
		t = 0.99α	0.9888	25,500	19%	1.69
		t = 0.95α	0.9488	5,800	4%	0.35
R200	1256.6	t = α	0.9574	143,800	100%	∞
		t = 0.99α	0.9478	128,900	98%	19.70
		t = 0.95α	0.9095	90,650	76%	8.60

In designing a resonator to closely meet the critical coupling requirement of t = α, one needs prior knowledge of the waveguide loss, the fabricated waveguide width and gap size as

#97938 - $15.00 USD Received 25 Jun 2008; revised 30 Aug 2008; accepted 8 Sep 2008; published 11 Sep 2008

compared to the design values, and it is difficult to achieve better than 5% accuracy in these measurements. Effects such as the additional coupling from the curved portion of the ring cavity also need to be taken into account, and they often require empirical calibrations. For example, the coupler length should be 1.3 μm for a R5 ring using a gap size of 0.45 μm. If the final (effective) coupler length is 2 μm, this causes a change of 1% in t. Using the same gap size, the required coupler length is 7.6 μm for a R200 ring, and the same variation in the coupler length causes a 0.8% change in t. The Si thickness is another variable, which can easily depart by ±3% from the manufacture specified value. On the other hand, for a given coupler gap size, the effect of gap variation on Q is independent of the cavity length, since a longer cavity ring also requires a longer coupler section. Considering all these factors and the properties of both Q and η, it is beneficial to use a longer cavity in order to achieve reproducible high quality factors and high contrasts ratios for reliable sensor measurements. A longer cavity comes with a reduced FSR, a consequence which may not be acceptable in applications such as telecommunications. For sensing measurements, the constraints on FSR are much less demanding. It should also be noted that if the waveguide loss is large, the transmitted signal I_{max} and the resonance amplitude (I_{max}-I_{min}) eventually diminishes with increasing L, rendering the resonator no longer useful. This sets a limit for the maximum L that can be used.

3. Experiment

We have fabricated sensor devices on SOI wafers having a 260 nm thick silicon layer on a 2 μm thick BOX layer, using different cavity designs. Figure 4 shows a simple race-track cavity, a spiral and a switch-back geometry. The spiral and switch-back resonators in Fig. 4(b, c) have cavity lengths of ~1.2 mm using 5 μm minimum bend radius and 10 μm waveguide separations, and are fitted into a < 110 μm × 110 μm area, and they showed similar performance. These designs are still conservative, and the footprint can be made smaller by using smaller waveguide separations. Waveguides of 450 nm wide were patterned by e-beam lithography using NEB22 photoresist and etched in an inductively coupled plasma (ICP) RIE system using a C_4F_8/SF_6 chemistry. Inverse tapers down to 150 nm in width were adopted at both the input and output facets to improve the waveguide to fiber coupling efficiency, and the estimated fiber to waveguide coupling loss is ~ 3 dB per facet [19]. The overall device is 5-6 mm long from facet to facet, including the access waveguides. To isolate the optical mode of the non-sensing regions of the device from the environment, a 2 μm thick layer of SU-8 polymer was spun on the wafer and windows were opened over the active sensing area using optical contact lithography. The devices were then baked at 200 °C for 60 minutes to cure the film. Finally, samples were exposed to an O_2 plasma to remove any residual photoresist in the sensor windows as well as to oxidize the silicon surface to form the desired oxide layer of approximately 3 nm in thickness for later functionalization.

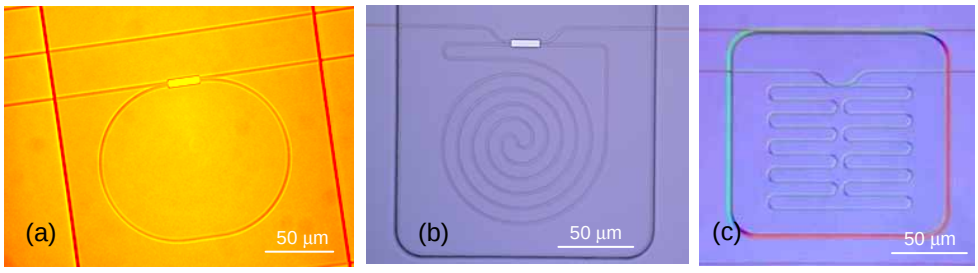

Fig. 4. Top view optical images of the fabricated silicon wire ring resonators with the sensing windows opened in the SU8 layer. (a) Simple race-track ring with L=336 μm; (b) Spiral ring with an MMI coupler and L= 1.27 mm; (c) Switch-back ring with a directional coupler.

#97938 - $15.00 USD Received 25 Jun 2008; revised 30 Aug 2008; accepted 8 Sep 2008; published 11 Sep 2008

The devices were tested using a tunable laser coupled to the input facet via a polarization maintaining tapered fiber. An objective of 10 × magnification was used on the output side to collect the transmitted signal. The measurements were performed in lab ambient without temperature control, with a typical temperature fluctuation of 0.2°C per 10 min. For waveguides with air cladding, which is the most temperature sensitive among the Si waveguides under the different cladding materials involved, the measured thermo-shift is ~ 55 pm/°C. We have tested resonators excited using either a directional coupler or a multi-mode-interference (MMI) coupler, and with different cavity lengths. The resonators shown in Figs. 4(a), 4(b) use MMI couplers of 3 μm × 9 μm in size and with a 50:50 power splitting ratio. Compared to the conventional ring resonators based on directional couplers (Fig. 4(c)), the MMI-based resonators have more relaxed fabrication requirements [18, 21] and are relatively insensitive to cladding material or fluid composition variations. There is a decrease in the Q due to over-coupling, but the penalty is acceptable for long cavity rings. Figure 5 shows the transmission spectra of the race-track cavity ring shown in Fig. 4(a) (L = 336 μm, R = 50 μm), and the spiral cavity resonator shown in Fig 4(b) (L = 1.27 mm, equivalent to R ~ 200 μm). The race-track resonator has a quality factor of Q ~ 6,000 and an extinction ratio of ~ 8 dB. The spiral resonator has an overall insertion loss of approximately -9dB, which includes the fiber-to-waveguide coupling loss and on-chip loss. The quality factor Q is ~ 19,600 and the extinction ratio is approximately -25 dB, even though the spiral ring contains bends with 5 μm minimum radius. The smaller insertion loss for the spiral ring is due to small variations in the fiber-to-waveguide coupling efficiency, and not an intrinsic difference between the two resonator designs. The variations in Q for the spiral rings are typically better than 10%, while the R5 and R50 rings are much more variable.

The measured quality factors for these two ring resonators are compared in Fig. 3(c) with theoretical predictions for resonators with a constant coupling ratio of t = 0.707. This coupling ratio is close to the data extracted from the measured resonance spectra. The measured Q values are lower than predicted assuming a ring waveguide loss scaling factor of s = −3 dB/cm, but agree reasonably well for s = −22 dB/cm. From our loss measurements on straight waveguides using the Fabry-Perot method, the propagation loss was estimated as ~ −3 dB/cm. These results suggest that there are other sources contributing to the cavity loss. We have analyzed rings with different cavity lengths in simple race-track, spiral and switch-back configurations, which consist of cavities using different bend radii. The loss factor α was found to decrease with L linearly to a reasonable approximation, and the difference between the spiral and switch-back rings is not obvious, even though the two designs contain different counts of 5 μm radius bends. These results suggest that the bend loss is negligible. The coupler loss α_C, as extracted from the intercept of the linear dependence between α and L, is also insignificant. On the other hand, a loss of −22 dB/cm can not be attributed only to the waveguide propagation loss, since the measured device has a total length of ~ 6mm and a total insertion loss of −9 dB, and the fiber-to-waveguide coupling loss was measured as approximately −3dB per facet. Similar cavity loss levels have been observed in other work [22]. The underlying cause for these apparent discrepancies in our devices is still under investigation. Nonetheless, the trend of Q increasing with L is clear, verifying the relation predicted by Eq. (2).

#97938 - $15.00 USD Received 25 Jun 2008; revised 30 Aug 2008; accepted 8 Sep 2008; published 11 Sep 2008

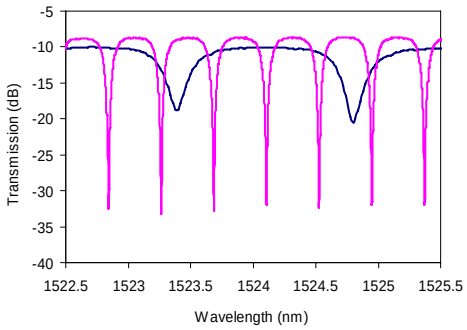

Fig. 5. Measured transmission spectra for the simple race-track ring (blues line) and the spiral ring (magenta line), which are shown in Fig. 4(a, b).

To investigate the sensing response to molecular surface adsorption, we used the biotin-streptavidin system, since it provides a well understood and irreversible binding affinity reaction. The oxide surface of the sample was functionalized with a silane chemistry in order to immobilize the vitamin biotin. A cleaned surface was silanized with 3-aminopropyltriethoxysilane (APTES) vapor and then rinsed with ethanol and dried. Next, the surface was biotinylated in a solution of N-hydroxysuccinimide (NHS) activated biotin in dimethylformamide (DMF) followed by rinsing with DMF and ethanol. The same functionalization procedure was repeated on a blanket silicon witness sample with an oxide covering layer, which was used for ellipsometry measurements to monitor the functionalization process. The witness samples was immersed for one hour in a streptavidin solution of 100 μg/ml diluted in phosphate buffered saline (PBS), then rinsed in PBS and dried. The thickness of the streptavidin layer at saturation was measured as $d \approx 1.8$ nm, assuming a layer refractive index of 1.46 at 633 nm wavelength. Given that the streptavidin molecule has a size of $4.5\times4.5\times5.8$ nm^3 [23], we estimate that the final surface coverage of the streptavidin molecules is approximately 40% (=1.8/4.5) of a close packed monolayer. Random sequential adsorption model predicts that the achievable packing density is < 60% for hard spheres binding at random to a surface. With the molecular weight of 60 kDa (or 9.96×10^{-20} g) for streptavidin and assuming a binding area of $4.5\times5.8 \approx 26$ nm^2, the mass density at saturation is estimated as ~ 1.6 ng/mm^2 and the total mass for the spiral sensor with a total surface area of 1232 μm^2 (including the top and sidewalls) is ~ 2 pg.

A molded PDMS sheet with microfluidic channels for sample fluid delivery was aligned with the ring resonator sensor elements and pressure bonded onto the sensor die. The ring resonance wavelength was monitored continuously by repeatedly scanning the laser wavelength over a 3 nm wavelength range. Each scan took approximately five seconds. A PBS solution was first injected in the microfluidic channel, followed by streptavidin diluted in the PBS solution. The symbols in Fig. 6(a) shows the resonance wavelength shifts as a function of time for the spiral cavity ring resonator shown in Fig. 4(b), with the injection of streptavidin of increasing concentrations of 0.1, 1 and 10 μg/ml in PBS. The slope of change for $\Delta\lambda$ increases approximately ten fold with each consecutive solution, consistent with the streptavidin concentration increase. After the injection of the 10 μg/ml solution, the surface approaches saturation and the total resonance wavelength shift approaches 0.63 nm. The transmission spectra at 0, 100, 300 and 400 sec are shown in Fig. 6(b), showing well resolved shifts with minimum change in the transmission notch profile.

Assuming the streptavidin surface density at saturation for the sensing sample exposed to streptavidin by microfluidics transport is the same as that for witness sample by static immersion, then the estimated mass density is ~ 1.6 ng/mm^2 at saturation, and the sensing response of $\Delta\lambda = 0.63$ nm can be converted to 1.5 fg/pm, or 2.5 pg/mm^2·pm. The wavelength shift data for the injection of each solution concentration is converted to the mass density

#97938 - $15.00 USD Received 25 Jun 2008; revised 30 Aug 2008; accepted 8 Sep 2008; published 11 Sep 2008

values and the results are plotted in Fig. 7 as a sensorgram. Note that the surface was not regenerated between the injections of consecutive solutions. Considering the RMS noise level shown in the insert of Fig. 7 as the minimum detectable wavelength shift, we estimate that this spiral ring resonator can resolve adsorptions as small as a mass density of 3 pg/mm^2. This limit of detection (LOD) compares favorably with commercial SPR instruments with temperature stabilization, which have a typical detection limit of 1-5 pg/mm^2 [24]. The mass density limit corresponds to a total mass of ~ 4 fg if both the waveguide top and sidewall surfaces are included (total of 1232 μm^2). This is an underestimate of the mass LOD, since the sidewalls have a much smaller contribution to the sensing signal.

The measured binding data was used for the kinetics analysis of molecular interaction. The streptavidin-biotin bond is known to have very high association rate constant of $\kappa_a = 7.5\times10^7$ $M^{-1}s^{-1}$ [25]. The measured response of the sensor is much slower than what is predicted from the Langmuir model of adsorption limited kinetics of streptavidin-biotin binding, suggesting the rate is limited by mass transport as expected. Figure 6(a) compares the measured response with calculations from the adsorption-limited Langmuir model and the two-compartment model. The two-compartment model combines the kinetics of absorption and desorption with an approximate treatment of transport through a diffusive boundary layer [26]. If B is the surface density of bound streptavidin, R_T the maximum surface density, C_T the concentration of streptavidin in the bulk solution, and C_i the concentration near the surface (in the so-called 'inner compartment', which has a thickness h_i), then:

$$\frac{dB}{dt} = \kappa_a C_i (R_T - B) - \kappa_d B \tag{5}$$

$$\frac{dC_i}{dt} = \frac{1}{h_i}(\kappa_m (C_T - C_i) - \frac{dB}{dt}) \tag{6}$$

Here κ_a and κ_d are the association and the dissociation rate constant respectively, and κ_m the mass transport constant. The curve labeled 'Langmuir model' in Fig. 6(a) shows the response expected if κ_m is large (no mass transport limit), using $\kappa_a = 7.5\times10^7$ $M^{-1}s^{-1}$ [25] and neglecting κ_d to reflect the strong affinity between streptavidin and biotin. R_T is taken to be $R_T = 2.5\times10^{11}$ M m from the ellipsometry results of 40% surface coverage, and assumed to correspond to 0.63 nm in wavelength shift. The curve labeled 'Two-compartment model' shows the result for a value $\kappa_m = 1.6\times10^{-6}$ m s^{-1} chosen to fit the data (The results are insensitive to the value of h_i). The agreement shows that the two-compartment model can explain the data qualitatively, supporting the idea that the response is mass-transport limited, although the value of κ_m is several times smaller than expected from the geometry of the sensor device. Accurate determination of κ_m requires knowledge of the chemical properties of not only the active Si sensing surface, but also the SU8 and PDMS surfaces in our sensors and the possibility of analyte uptake, and this information is currently still insufficient. However, these results show that these sensors can be used for molecular binding kinetics analysis, a key feature of this label-free and real-time sensing technique.

#97938 - $15.00 USD Received 25 Jun 2008; revised 30 Aug 2008; accepted 8 Sep 2008; published 11 Sep 2008

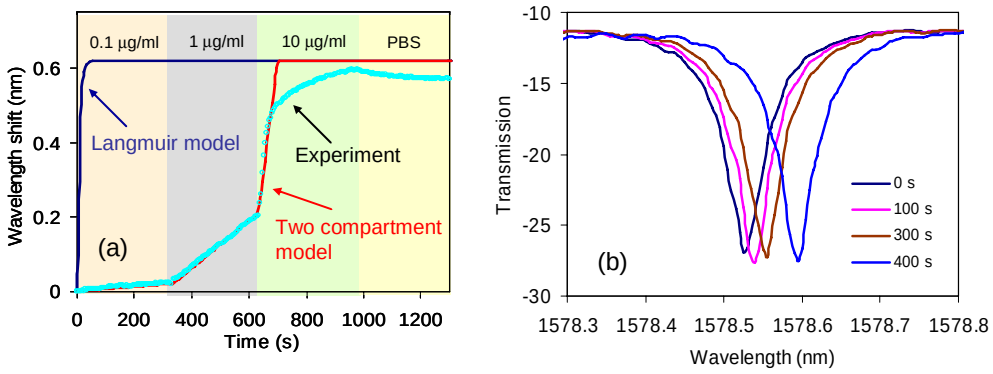

Fig. 6. (a). Measured spiral ring resonator resonance wavelength shift $\Delta\lambda$ as a function of time during PBS and streptavidin exposure. During this experiment, the streptavidin concentration was increased from 0.1 µg ml^{-1} to 1 µg ml^{-1} and then to 10 µg ml^{-1}, with a corresponding increase in the signal slope; (b) Measured transmission spectra at the following time: 0, 100, 300 and 400 sec.

4. Summary

We have described our work in developing a high sensitivity ring resonator biological sensor with improved fabrication tolerance, using a long resonator cavity made of densely folded silicon photonic wire waveguides. For practical implementation of ring resonator sensors, large response to surface binding events, high quality factor, significant resonance contrast and robust performance are all important considerations. Taking advantage of the high index contrast in SOI waveguides, a strong optical field localized near the surface is obtained by miniaturizing the waveguide cross-section, thus giving a large response to the surface adsorption. The quality factor of ring resonators are shown to increase with the cavity length L for a given waveguide loss per unit length. A lengthened cavity relaxes the critical coupling condition and provides stable resonance contrast and high quality factors which are only weakly affected by loss or coupling variations. This feature is beneficial for multiple sensor arrays where the reference and the sensing elements are required to be nominally identical. Long sensor interaction lengths of over 1.27 mm fitted within a small area of 110µm × 110µm are achieved with a Q of ~20,000 by using small bending radii, providing compatibility with spotter functionalization, microfluidic sample delivery and sensor arraying. Measurements of surface adsorption of protein molecule are presented using the biotin-streptavidin binding system. Binding events in streptavidin solutions as dilute as 0.1 µg/ml (or 1.7 nM) were detected, with a resolvable mass density 3 pg/mm^2 or a total mass of ~5 fg. The binding data was used for kinetics analysis of molecular interaction. The results show qualitative agreement with the two-compartment model, indicating that the measured reaction rate is transport limited. This real time detection of low analyte concentrations, together with robust performance and a remarkable reduction in sensor footprint achieved using silicon wire waveguide sensors are important advances towards the development of optical lab-on-chip molecular sensing, particularly for sensor arrays based on waveguide evanescent field transduction.

#97938 - $15.00 USD Received 25 Jun 2008; revised 30 Aug 2008; accepted 8 Sep 2008; published 11 Sep 2008

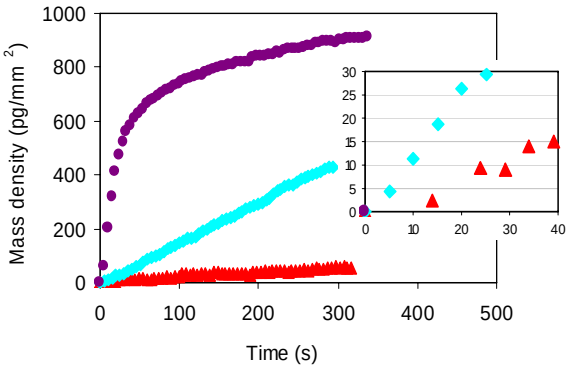

Fig. 7. Measured molecular binding signal in terms of surface mass density as a function of molecular exposure time. The data are converted from the results shown in Fig. 6(a), and the insert shows the data for the first 40 sec.

#97938 - $15.00 USD Received 25 Jun 2008; revised 30 Aug 2008; accepted 8 Sep 2008; published 11 Sep 2008